RAA 2015 Vol. **15** No. **4**, 569–582 doi: 10.1088/1674–4527/15/4/009
http://www.raa-journal.org *http://www.iop.org/journals/raa*

***R**esearch in*
***A**stronomy and*
***A**strophysics*

Characterizing motion types of G-band bright points in the quiet Sun *

Yun-Fei Yang[1,2,3], Hui-Xue Qu[1], Kai-Fan Ji[1], Song Feng[1,2,3], Hui Deng[1], Jia-Ben Lin[2] and Feng Wang[1,4†]

[1] Faculty of Information Engineering and Automation / Yunnan Key Laboratory of Computer Technology Application, Kunming University of Science and Technology, Kunming 650500, China; *yfyangkmust@gmail.com*
[2] Key Laboratory of Solar Activity, National Astronomical Observatories, Chinese Academy of Sciences, Beijing 100012, China
[3] Key Laboratory of Modern Astronomy and Astrophysics, Nanjing University, Ministry of Education, Nanjing 210093, China
[4] Yunnan Observatories, Chinese Academy of Sciences, Yunnan 650011, China

Received 2014 April 28; accepted 2014 July 29

Abstract We study the motion of G-band bright points (GBPs) in the quiet Sun to obtain the characteristics of different motion types. A high resolution image sequence taken with the *Hinode*/Solar Optical Telescope (SOT) is used, and GBPs are automatically tracked by segmenting 3D evolutional structures in a space-time cube. After putting the GBPs that do not move during their lifetimes aside, the non-stationary GBPs are categorized into three types based on an index of their motion type. Most GBPs that move in straight or nearly straight lines are categorized as a straight motion type, a few moving in rotary paths into rotary motion, and the others fall into a motion type we called erratic. The mean horizontal velocities are $2.18\pm0.08\,\mathrm{km\,s^{-1}}$, $1.63\pm0.09\,\mathrm{km\,s^{-1}}$ and $1.33\pm0.07\,\mathrm{km\,s^{-1}}$ for straight, erratic and rotary motion types, respectively. We find that a GBP drifts at a higher and constant velocity during its whole life if it moves in a straight line. However, it has a lower and variational velocity if it moves on a rotary path. The diffusive process is ballistic-, super- and sub-diffusion for straight, erratic and rotary motion types, respectively. The corresponding diffusion index (γ) and coefficients (K) are 2.13 ± 0.09 and $850\pm37\,\mathrm{km^2\ s^{-1}}$, 1.82 ± 0.07 and $331\pm24\,\mathrm{km^2\ s^{-1}}$, and 0.73 ± 0.19 and $13\pm9\,\mathrm{km^2\ s^{-1}}$. In terms of direction of motion, it is homogeneous and isotropic, and usually persists between neighboring frames, no matter what motion type a GBP is classified as.

Key words: techniques: image processing — Sun: photosphere — methods: data analysis — methods: statistical

∗ Supported by the National Natural Science Foundation of China.
† Corresponding author

1 INTRODUCTION

Photospheric bright points moving in intergranular dark lanes are clearly visible in G-band observations, and are often referred to as G-band bright points (hereafter GBPs). Recent studies show that the motion of GBPs is mainly determined by the buffeting motion of granules. The convective motions of granules violently push and squeeze GBPs, resulting in chaotic motion of GBPs (Berger et al. 1998a; van Ballegooijen et al. 1998; Möstl et al. 2006; Giannattasio et al. 2013; Keys et al. 2014). These small-scale motions are thought to play an important role in heating the upper solar atmosphere by twisting and braiding magnetic flux tubes, generating kinetic energy, Alfvén waves and so on (Cranmer 2002; Cranmer & van Ballegooien 2005; Klimchuk 2006; de Wijn et al. 2009; Zhao et al. 2009; Balmaceda et al. 2010).

High resolution observations have led scientists to study the motions of GBPs. Results show there are mean horizontal velocities of 1–2 $\mathrm{km\ s^{-1}}$ with maximum values of 7 $\mathrm{km\ s^{-1}}$ (Muller et al. 1994; Berger et al. 1998b; Möstl et al. 2006; Utz et al. 2010; Keys et al. 2011). Isolated GBPs move fast at birth, then decrease to their lowest velocities in the middle stage of their lifetime, and then they accelerate again in the decay stage until their eventual disappearance (Yang et al. 2014). The direction of motion usually persists from one time interval to the next (Nisenson et al. 2003; Bodnárová et al. 2014).

The random motion of a GBP is commonly described in terms of turbulence. One important component of turbulence is diffusion, where the dispersion mechanism is defined by the diffusion index (γ) and the efficiency of this mechanism is given by the diffusion coefficient (K). Earlier studies interpreted their results as indicative of normal- or sub-diffusive processes (Berger et al. 1998a; Cadavid et al. 1999). However, recent studies, both using G-band images and magnetograms from ground and space observations, agree on a super-diffusive dynamic regime with a γ of $1.2 - 1.7$ (Abramenko et al 2011; Chitta et al. 2012; Giannattasio et al. 2014; Jafarzadeh et al. 2014; Keys et al. 2014). The diffusion coefficient measures the rate of increase in the dispersal area in units of time. The values reported in previous literatures lie between 0.87 $\mathrm{km^2\ s^{-1}}$ and 350 $\mathrm{km^2\ s^{-1}}$ (Berger et al. 1998a; Utz et al. 2010; Manso Sainz et al. 2011; Giannattasio et al. 2014; Jafarzadeh et al. 2014).

Another component of turbulence is vortex motion. Vortices occurring in simulations have been suggested as a primary candidate mechanism, with roots in the photosphere, for energy transport from the solar interior to the outer layers of the solar atmosphere (Vögler et al. 2005; Carlsson et al. 2010; Fedun et al. 2011; Moll et al. 2011; Shelyag et al. 2011; Shelyag et al. 2013). Shelyag et al. (2011) simulated G-band images and showed a direct connection between magnetic vortices and rotary motions of photospheric bright points, and suggested that there may be a connection between the magnetic bright point rotation and small-scale swirl motions observed higher in the atmosphere. Vortex-type motions have also been measured by tracking bright points in high-resolution observations of the photosphere. Bonet et al. (2008) traced the motions of bright points which follow spiral paths on the way to being engulfed by a downdraft. Goode et al. (2010) noted that colliding granules create a vortex into which the encircled bright points enter and spin around each other. Additionally, Wedemeyer-Böhm et al. (2012) demonstrated, using a series of co-spatial images at different atmospheric layers, that "magnetic tornadoes" in the chromosphere and transition region result in rotational motions of the associated photospheric bright points.

Although the motions of GBPs are chaotic (Nisenson et al. 2003; Möstl et al. 2006; Chitta et al. 2012), it seems that there are some typical motion types, such as straight motion, rotary motion and so on. However, studies focusing on motion types of GBPs are relatively scarce. For exploring the characteristics of different motion types, we designed a classification method and categorized motions of GBPs into three types: straight, erratic and rotary motions. The characteristics in terms of horizontal velocity, diffusion and direction of motion of different motion types were measured and compared. The layout of the paper is as follows. The observations and data reduction are described

in Section 2. The classification method is detailed in Section 3. In Section 4, the characteristics of different motion types are presented. Finally, the discussion and conclusion are given in Section 5.

2 OBSERVATIONS AND DATA REDUCTION

A series of G-band images was obtained between 18:19 UT and 20:40 UT on 2007 February 19 with the Solar Optical Telescope (SOT; Ichimoto et al. 2004; Suematsu et al. 2008) onboard the *Hinode* satellite. The field-of-view (FOV) was $27.7'' \times 27.7''$ with a pixel size of $0.054''$. The telescope was pointed at a quiet region at the disk center. There are 758 frames over a period of roughly $2\,\mathrm{h}$ and $20\,\mathrm{min}$ with a temporal sampling of $11\,\mathrm{s}$. The level-0 data sequence was calibrated and reduced to level-1 using the standard data reduction algorithm fg_prep.pro distributed in Solar Software.

Since our intention is to study the motions of GBPs, we designed a highly accurate solar image registration procedure based on a cross-correlation method to correct the satellite drift. It includes seven steps: (1) apply a Tukey window as an apodization function on both reference image $f(x, y)$ and image undergoing registration $g(x, y)$; (2) calculate the cross-power spectrum that is defined as: $R(u, v) = F(u, v) * G(u, v)$, where $F(u, v)$ and $G(u, v)$ are the Fourier transform of $f(x, y)$ and $g(x, y)$ respectively, and $*$ denotes the complex conjugate operation; (3) obtain the centralized cross-correlation surface $r(x, y)$ by applying an inverse Fourier transform to $R(u, v)$ and centering the zero-frequency component; (4) locate the peak in $r(x, y)$, then measure the distances between the peak and the center of $r(x, y)$, which are the pixel-level displacements of the horizontal and vertical components between $f(x, y)$ and $g(x, y)$; (5) shift $g(x, y)$ over the pixel-level displacements, then repeat steps 1 – 4 until the displacement is below one pixel; (6) determine the sub-pixel displacements by measuring the centroid of the peak in $r(x, y)$, the modified moment method is applied and the threshold is selected by the minimum value of a small circle surrounding the peak; (7) shift $g(x, y)$ over the sub-pixel displacements by the bicubic interpolation method.

The algorithm is based on the assumption that the maximum of the peak is at the same position as the centroid. It implies the correlation value above the threshold should be symmetrical in the horizontal and vertical directions. This assumption is only acceptable in a very small central area around the cross correlation peak. Our simulated experiment shows that the alignment accuracy produced by this procedure can be as high as 0.02 pixels between two neighboring frames if we set the radius of the circle as two pixels. After image alignment, the overlap of the FOV in the sequence is $20.5'' \times 20.5''$ (380 pixel$\times$380 pixel).

The Laplacian and Morphological Dilation algorithm described in Feng et al. (2012) was used to detect GBPs in each image, and the three-dimensional (3D) segmentation algorithm described in Yang et al. (2014) was employed to track the evolution of GBPs in the image sequence.

A 3D space-time cube (x, y, t) is modeled where the $\boldsymbol{x}$ and $\boldsymbol{y}$ axes are the two-dimensional image coordinates, and the t axis represents the frame index or the time-slice of the image sequence. The 3D structures in the space-time cube represent the evolution of GBPs. Figure 1 shows a segment of the 3D space-time cube whose size is 380 pixel$\times$380 pixel$\times$46 min. A possible chaotic outcome is very similar to previous simulations of photospheric turbulent convection and evolution of magnetic footpoints (Carlsson et al. 2010; Moll et al. 2011; Shelyag et al. 2012; Wedemeyer-Böhm et al. 2012). It can be seen that these GBPs have different motion types during their lifetimes. For instance, some GBPs move in nearly straight lines in different directions and some move in somewhat circular paths. It is worth noting that not only twisted but also braided GBPs can be found in this cube.

3 CLASSIFICATION OF MOTIONS

Although the motions of GBPs look random, there are some typical types. To explore the characteristics of different motion types, we designed a method to classify the motions.

Initially, some GBPs were discarded in order to reduce statistical error before classification. A GBP is discarded if (1) its equivalent diameter is smaller than $100\,\mathrm{km}$ or larger than $300\,\mathrm{km}$, (2) its

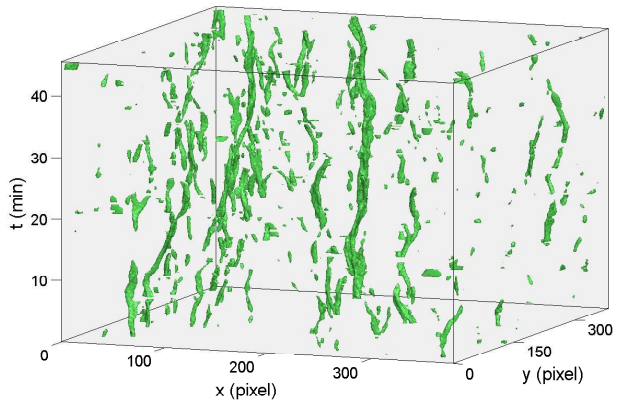

Fig. 1 A segment of the 3D space-time cube whose size is 380 pixel×380 pixel×46 min. The x and y axes are the two-dimensional image coordinates, and the t axis represents frame index or the time-slice of the image sequence. It can be seen that the GBPs move in different motion types.

lifetime is shorter than 55 s, (3) its velocity exceeds 7 $\mathrm{km\ s^{-1}}$, (4) its life cycle is not complete or (5) if merging or splitting occurs during its lifetime. As a result, a total of 753 3D evolving structures remain.

Next, we put stationary GBPs, or those that have limited motion during their lifetimes, aside to measure the dynamics of the GBPs in detail. Projecting the 3D evolving structures onto the two-dimensional (x, y) space, the path of each GBP can be described respectively by a sequence of centroid coordinates $(X(t), Y(t))$ of the GBP in each frame, t. Bodnárová et al. (2014) defined a rate of motion as $m = d/r$, where d is the displacement over the lifetime of a GBP, as $d = \sqrt{(X(n) - X(1))^2 + (Y(n) - Y(1))^2}$; here 1 is the start frame and n is the final frame during its lifetime; r is the radius of the circle which corresponds to the size of the GBP at its start location. Bodnárová et al. (2014) regarded about 45% of the GBPs that were tracked as stationary GBPs with $m < 1$. However, if a GBP moves in a large circular path, and its start location is very close to its final location, the value d will be very small. This could result in misjudging it as a stationary GBP. Hence, to address this issue, we revised the rate of motion as $m' = d'/r'$, where $d' = \sqrt{(X_{\max} - X_{\min})^2 + (Y_{\max} - Y_{\min})^2}$. Here $X_{\max}$ and $X_{\min}$ are the maximum and minimum coordinates of the path of a single GBP along the $\boldsymbol{x}$ axis, and $Y_{\max}$ and $Y_{\min}$ are those along the $\boldsymbol{y}$ axis; r' is the radius of a circle which corresponds to the maximum size of the GBP during its lifetime. The d' value may more realistically represent its actual range of motion. All m' values of GBPs were calculated and about 43% of them are below 1, which means their range of motion is smaller than their own maximum radius. About 25% are greater than 2, which means that these GBPs show significant movement. The maximum value of m' is 7.5. As a result, a total of 324 GBPs with $m' < 1$ were regarded as stationary GBPs. The remaining 429 GBPs with $m' \geq 1$, called non-stationary GBPs, were included in the classification of motion types.

Finally, we classified non-stationary GBPs into three motion types. An index of motion type, mt, is defined as $mt = d/L$, where d is the displacement defined as above; L is the whole path length, defined as $L = \sum_{t=1}^{n} \sqrt{\triangle X(t)^2 + \triangle Y(t)^2}$, where $\triangle X(t) = X(t+1) - X(t)$ and $\triangle Y(t) = Y(t+1) - Y(t)$. The index of motion type is a ratio of the displacement of a GBP to its whole path length.

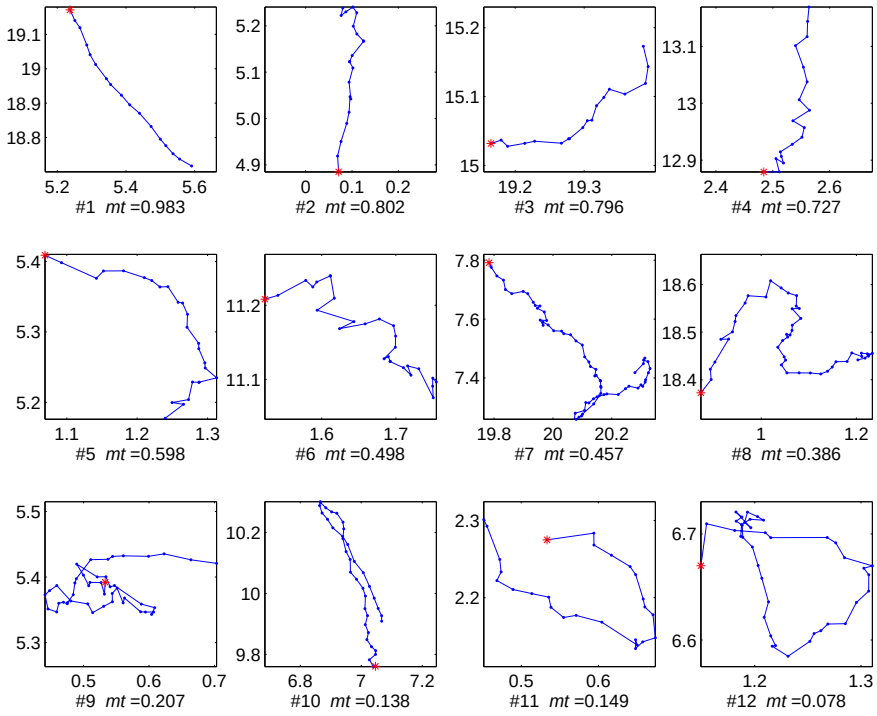

Fig. 2 The paths of twelve individual GBPs with corresponding mt. The starting position of each path is indicated by a red star. The x and y coordinates are ticked in arcsec.

According to the definition, mt is between 0 and 1. If a GBP moves in a nearly straight line, then mt will be close to 1. If it moves in a nearly closed curve, then mt will be close to 0. In our data set, the maximum mt is 0.996 and the minimum is 0.078.

Figure 2 shows the paths of twelve individual GBPs with corresponding mt. It can be seen that GBP # 1 and # 2 move in nearly straight lines, and their mt values are 0.983 and 0.802 respectively. However, GBP # 11 and # 12 trace almost closed curves, and their mt values drop to 0.149 and 0.078, respectively. All paths that the GBPs follow are very similar to previous studies (Nisenson et al. 2003; Möstl et al. 2006; Chitta et al. 2012). However, we have not found a spiral path similar to those reported by Bonet et al. (2008).

Figure 3 shows the Probability Density Function (PDF) of mt and the best exponential fit. The mt value of 50% for GBPs is larger than 0.83 and 15% of GBPs have an mt value of less than 0.5. That means most GBPs move in straight or nearly straight lines, and only a few GBPs move along rotary paths. Focusing on straight motion and rotary motion, we classified the motions into three types: straight, erratic and rotary. A GBP that moves in a straight or nearly straight line is classified as the straight motion type, and a GBP that traces a closed or almost closed curve is classified as the rotary motion type. If the path of a GBP is neither straight nor rotary, it will be categorized into the erratic motion type. The erratic motion type is more like a transition between the straight and the rotary type. Considering the exponential distribution of mt, and checking individual GBPs, we set one threshold between straight and erratic motion of mt at a value of 0.8 and another between erratic and rotary motion at a value of 0.4. The threshold of 0.8 is reliable for distinguishing the straight motion type. However, the threshold of 0.4 is a compromise. The lower the threshold of mt is, the clearer the rotary motion of the GBP is. Unfortunately, the quantity of GBPs with low mt is very

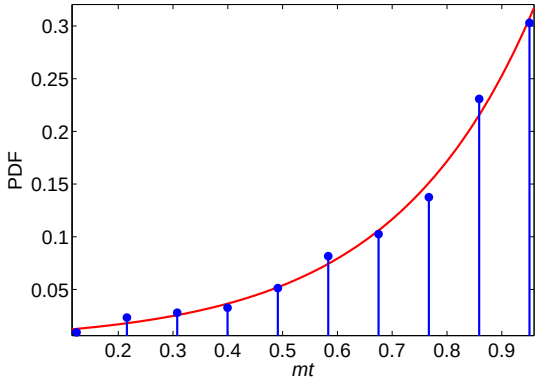

Fig. 3 The distribution of mt. The PDF of mt is drawn in blue. The red solid line is the exponential fit.

small. If we set a very low threshold, the statistical results would be meaningless. Consequently, 54% of GBPs (232 GBPs) were categorized as having straight motions, about 7% (31 GBPs) had rotary motions, and the others were erratic in nature. Comparing the paths in different panels in Figure 2, we can see that the classification is consistent with our subjective understanding. Some special cases will be discussed in Section 5.

4 RESULTS

4.1 Horizontal Velocity

The horizontal velocity of a GBP between two neighboring frames can be calculated by $v = \sqrt{v_x^2 + v_y^2}$. The horizontal velocities of all the GBPs studied were calculated and the corresponding PDFs all follow Rayleigh distributions. Figure 4 shows the PDFs for the horizontal velocities of the different motion types in dotted lines and the corresponding curve fits for these are displayed as solid lines. The means and standard errors of velocities are $2.18\pm0.08\,\mathrm{km\ s^{-1}}$ for the straight motion type, $1.63\pm0.09\,\mathrm{km\ s^{-1}}$ for the erratic motion type and $1.33\pm0.07\,\mathrm{km\ s^{-1}}$ for the rotary motion type. For comparison, the PDF and Rayleigh fit for all motion types as a whole are drawn in black, with mean and standard error of $1.77\pm0.08\,\mathrm{km\ s^{-1}}$.

To quantify the difference between different motion types, we performed a two sample Kolmogorov-Smirnov (K-S) test between the distributions of straight and rotary motion types at the 5% significance level. The test result indicates that the difference in horizontal velocities between them is significant.

We also analyzed the correlation between the indices of motion type and horizontal velocities. The mean horizontal velocity of each GBP during its lifetime was calculated. Figure 5 shows the scatter diagram associated with the indices of motion type for 429 GBPs versus their mean horizontal velocities in black. Their mean values and associated standard deviations of the horizontal velocities were calculated separately and displayed in blue after all GBPs were divided into 10 equal bins. The best linear fit for the mean values is displayed as a red solid line. Additionally, we calculated the correlation coefficient between mt and the mean horizontal velocity, and obtained a value of 0.88. The results of classification and correlation analysis agree with one another, and both of them suggest that a GBP moving in a straight line has a higher velocity, and vice versa.

Furthermore, we quantified the evolution of GBPs for the different motion types in terms of velocity using a method described in Yang et al. (2014). The basis of the method is lifetime normal-

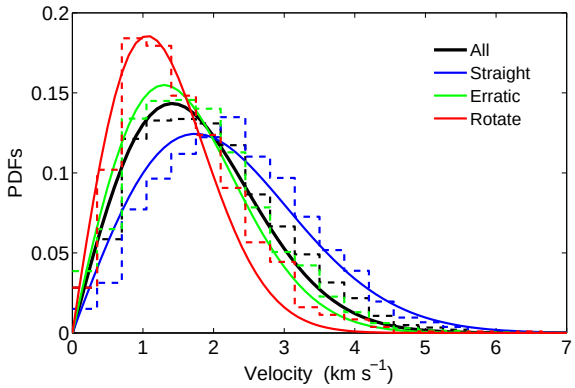

Fig. 4 The PDFs of straight, erratic and rotary motion types are shown in blue, green and red dotted lines, respectively. The PDFs are curve fitted with a Rayleigh curve, which is drawn with a solid line in the corresponding color. The means and standard errors of velocities are 2.18±0.08, 1.63±0.09 and 1.33±0.07 $\mathrm{km\ s^{-1}}$, respectively. In addition, the PDF and curve fit for all motion types as a whole are drawn in black, with mean and standard error of 1.77±0.08 $\mathrm{km\ s^{-1}}$.

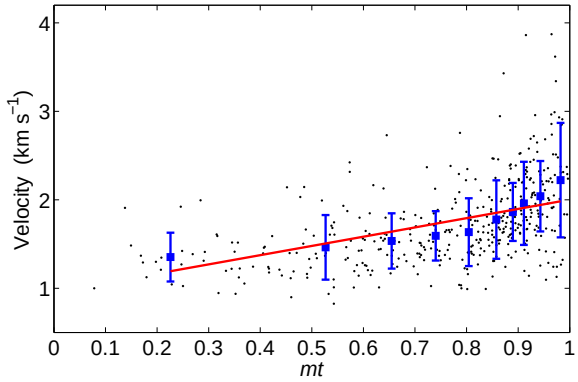

Fig. 5 The scatter diagram associated with the indices of motion type for 429 GBPs versus their mean horizontal velocities are drawn in black. All GBPs were divided into 10 equal bins. The mean values and associated standard deviations of velocity belonging to each bin are drawn in blue. The red solid line is the best linear fit for the means.

ization which standardizes different lifetimes to common stages. In general, dividing the life into five stages is representative of the entire evolution process, which can be described as birth, growth, middle, decay and disappearance. Significantly, the authors demonstrated that the GBPs have a similar evolutional pattern in terms of velocity, no matter how many stages the GBPs are divided into during their lifetime. Therefore, we divided the life of each GBP into five stages for different motion types. The PDFs of velocities in five stages are each separately fitted to a Rayleigh distribution. The means with associated standard errors are shown in Table 1. For comparison, the result of all motion types as a whole is listed. It can be seen that a GBP moving in a straight line not only has a higher velocity, but also has an almost constant velocity (about 2 $\mathrm{km\ s^{-1}}$). However, a GBP moving in a rotary path has a lower and varying velocity. On average, it moves relatively fast (1.36 $\mathrm{km\ s^{-1}}$) at birth, then

Table 1 Means and Standard Errors of the Velocity of GBPs Classified as Different Motion Types after Dividing Their Lives into Five Stages

Motion Type	Birth stage ($\mathrm{km\ s^{-1}}$)	Growth stage ($\mathrm{km\ s^{-1}}$)	Middle stage ($\mathrm{km\ s^{-1}}$)	Decay stage ($\mathrm{km\ s^{-1}}$)	Disappearance stage ($\mathrm{km\ s^{-1}}$)
Straight	2.17±0.13	2.16±0.13	2.16±0.12	2.17±0.14	2.18±0.13
Erratic	1.64±0.12	1.56±0.11	1.51±0.11	1.54±0.11	1.76±0.13
Rotary	1.36±0.18	1.21±0.16	1.20±0.16	1.29±0.17	1.58±0.21
All	1.83±0.08	1.72±0.08	1.61±0.08	1.77±0.08	1.86±0.09

decreases to its lowest velocity ($1.20\,\mathrm{km\ s^{-1}}$) in the middle stage, and accelerates again ($1.58\,\mathrm{km\ s^{-1}}$) in the decay stage until it disappears. Interestingly, Balmaceda et al. (2010) described a similar phenomenon when analyzing a series of images at different atmospheric layers. They reported the stochastic evolution of granules that allow the bright points to approach the region that the vortex influences, increase their velocities and eventually fall into the vortex.

4.2 Diffusion

Photospheric diffusion processes represent the efficiency of GBP dispersal in the photosphere, which can be characterized by the relation $\langle(\Delta l)^2\rangle = C\tau^{\gamma}$, where $\langle(\Delta l)^2\rangle$ represents the mean-squared displacement of the tracked GBP between its location at any given time τ and its initial position; γ is the diffusion index and C is a constant of proportionality. Motions with $\gamma < 1$, $\gamma = 1$ and $\gamma > 1$ are called sub-diffusive, normal-diffusive (random walk) and super-diffusive, respectively. Values for the squared displacement $(\Delta l)^2$ of the three motion types were calculated separately and illustrated in Figure 6 in different colors. Statistically, the behavior of all motion types as a whole is characterized by the scaling of the mean-squared displacement with time (represented by the dashed pink line). Only three GBPs can be traced beyond 600 s, so the extended tail of the mean-squared displacement is truncated to aid in the depiction of the diffusion index. The black line shows the best power fit with γ = 1.50±0.08 inside the time interval $11 - 600\,\mathrm{s}$, which displays significant super-diffusive behavior. Interestingly, most GBPs which move in straight lines have squared displacement above the fit line. These GBPs drift fast and have more Lévy flights, and they make a primary contribution to super or even ballistic diffusion ($\gamma = 2$). However, most GBPs which move in rotary paths have squared displacement below the fit line. They move slowly and contribute to a sub-diffusive regime.

We also calculated the mean-squared displacement for GBPs classified as straight, erratic and rotary motion types. We found values for γ of 2.13±0.09, 1.82±0.07 and 0.73±0.19 determined for time scales $\tau < 495\,\mathrm{s}$, $\tau < 600\,\mathrm{s}$ and $\tau < 550\,\mathrm{s}$, respectively. The mean-squared displacement $\langle(\Delta l)^2\rangle$ as a function of time, τ, of the three motion types are displayed in Figure 7 on a log-log scale. For comparison, the mean-squared displacement of all motion types as a whole is also drawn in Figure 7 with γ= 1.50.

The diffusion coefficient, K, representing the rate of area in unit time that a GBP moves across, is estimated as a function of time scale by Monin & Iaglom (1975), $K(\tau) = \frac{C\gamma}{4}\tau^{\gamma-1}$. In practice, C is the constant term of the equation $\langle(\Delta l)^2\rangle = C\tau^{\gamma}$, γ is the diffusion index and τ represents the lifetime of the GBP. As a result, K is 850±37 $\mathrm{km^2\ s^{-1}}$ for the straight motion type, 331±24 $\mathrm{km^2\ s^{-1}}$ for the erratic motion type and 13±9 $\mathrm{km^2\ s^{-1}}$ for the rotary motion type. Considering all motion types as a whole, K is 191±20 $\mathrm{km^2\ s^{-1}}$. The results for all three motion types are consistent with the results found for velocity and γ.

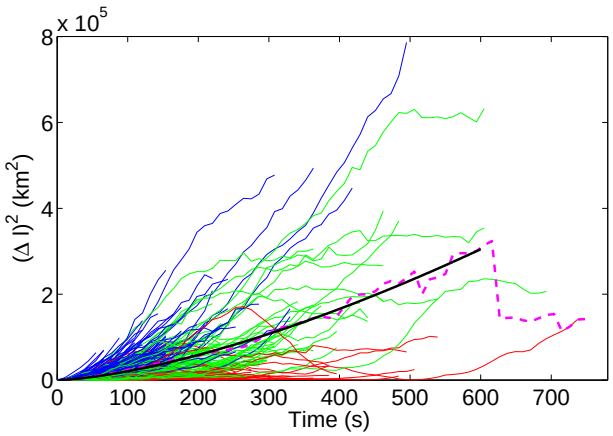

Fig. 6 The mean-squared displacements of straight, erratic and rotary motion types are shown in blue, green and red lines, respectively. The mean-squared displacement for all motion types as a whole, with time, is displayed as a dashed pink line. The black line shows the best power fit with γ = 1.50 for time scale $\tau < 600$ s, which is super-diffusive.

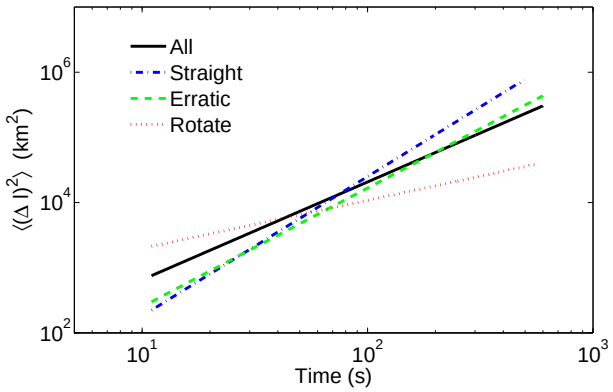

Fig. 7 Mean-squared displacement $\langle(\Delta l)^2\rangle$ as a function of time, τ, on a log-log scale. The best linear fits for straight, erratic and rotary motions are displayed in blue (*dash-dotted line*), green (*dashed line*) and red (*dotted line*), with γ = 2.13±0.09, 1.82±0.07 and 0.73±0.19, respectively. These are fitted for times $\tau < 495$ s, $\tau < 600$ s and $\tau < 550$ s, respectively. A solid line shows the best fit for all motion types as a whole in black, with γ = 1.50±0.08 for $\tau < 600$ s.

4.3 Direction of Motion

In order to explore whether GBPs drift in some preferential directions, a start-to-end direction angle is defined as the angle made by a given line (connecting sub-pixel centroids of the brightness of a GBP at its start location and its final location) with the reference axis. We calculated the start-to-end direction angle for each GBP belonging to the straight motion type. Figure 8 is the distribution of direction angles grouped into six bins. Obviously, the distribution does not show GBPs drifting in any preferential direction. Instead, their directions of motion are homogeneous and isotropic.

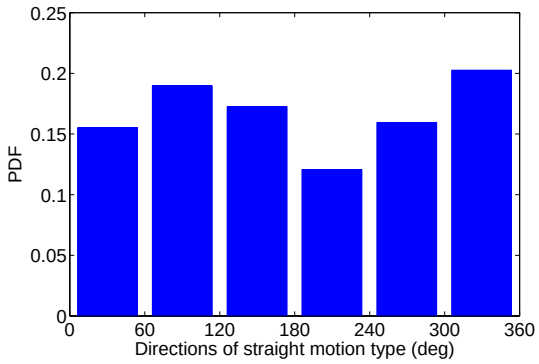

Fig. 8 The distribution of the start-to-end direction angle of GBPs for the straight motion type grouped into six bins. The x axis is ticked in degrees. The directions of motion are homogeneous and isotropic.

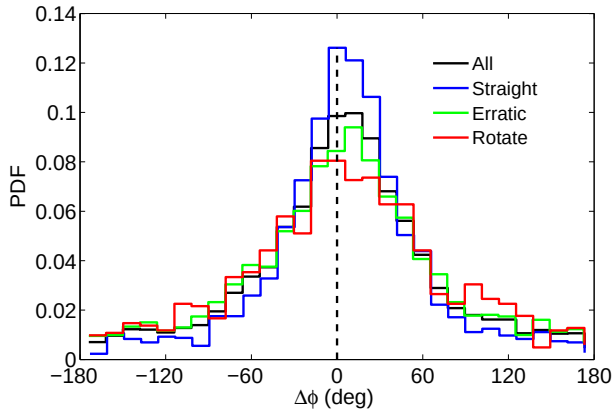

Fig. 9 The PDFs of $\Delta\Phi$ for straight, erratic and rotary motion type in blue, green and red, respectively. The black line shows the PDF for all motion types as a whole. The x axis is ticked in degrees.

In order to compare with previous studies (Nisenson et al. 2003; Bodnárová et al. 2014), we also measured the change of direction angle, $\Delta\Phi$, between neighboring frames. The PDFs of $\Delta\Phi$ of the different motion types are drawn in Figure 9. The fact that all distributions peak at 0 indicates that the direction of motion between neighboring frames varies very slowly. Since it is calculated using sub-pixel centroids, the direction of motion will only gradually change. However, the distributions of different motion types are not exactly the same. We employed kurtosis to measure the peakedness of the PDFs in Figure 9. Kurtosis is defined as follows

$$\text{kurtosis} = \frac{\frac{1}{n}\sum_{i=1}^{n}(x_i - \overline{x})^4}{[\frac{1}{n}\sum_{i=1}^{n}(x_i - \overline{x})^2]^2} - 3\,. \tag{1}$$

The kurtoses of straight, erratic and rotary motion types are 1.25, 0.17 and -0.11, respectively. The distribution of straight motion type is significantly leptokurtic (kurtosis$>$0), which has a narrower peak around the mean with thinner tails, and actually 54% of $\Delta\Phi$ are limited between -30° and 30°. However, the distribution of the rotary type is platykurtic (kurtosis$<$0), which has a lower

Table 2 Overview of Mean Velocities of GBPs in Previous Studies

Paper	Pixel size ($''$)	Temporal sampling (s)	Mean velocity (km s^{-1})
Muller et al. (1994)	0.25	20	1.33
Berger et al. (1998b)	0.4	23.75	1.47
Nisenson et al. (2003)	0.071	30	1.31
Möstl et al. (2006)	0.041	20	1.11
Keys et al. (2011)	0.069	2	$\sim$1
Utz et al. (2010)	0.054	11	1–2
Bodnárová et al. (2014)	0.071	30	0.89
This study	0.054	11	1.77

and wider peak around the mean with larger tails. Additionally, the kurtosis of all motion types as a whole is 0.42, which is slightly leptokurtic.

5 DISCUSSION AND CONCLUSIONS

We have analyzed the motions of isolated GBPs in the quiet Sun using a high resolution G-band image sequence acquired with *Hinode*/SOT. Although the motions of GBPs look random, they can be classified into different types. For exploring the motion of GBPs in detail, a rate of motion defined by Bodnárová et al. (2014) is revised as a ratio (m') of the real range of motion to the maximum radius of the GBP if we define it as having circular geometry. About 43% of GBPs studied displaying $m' < 1$ are discarded as stationary GBPs, which means that these GBPs do not move beyond their own boundaries during their lifetimes. The remaining 429 non-stationary GBPs are classified based on an index of motion type, mt, which is defined as a ratio of the displacement to the whole path length. The exponential distribution of these indices shows that most GBPs follow straight or nearly straight lines, with only a few moving in rotary paths. Consequently, we categorize the non-stationary GBPs into three types by imposing two subjective thresholds. About 54% of GBPs are categorized into a straight motion type, about 7% into a rotary motion type, and the others fall into a motion type we define as erratic.

Our classification method is simple but effective. It allows us to distinguish straight and rotary motions and allows us to explore the characteristics of different motion types. However, the motions of GBPs are very complicated, so the boundaries between these types are not quite clear. For example, GBP # 7 in Figure 2 moves in a straight line at first then has a circular path at the end of its lifetime. Considering its mt value and the proportion of the rotary motion along its whole path of motion, the erratic motion type is a suitable choice. Both GBP # 5 and # 11 move in open curved paths, but they are categorized into different types based on their displacement. In fact, the expansion and evolution of granules may result in the interruption of a rotary path of a GBP, so classifying a GBP with an open but clear curve into the rotary motion type might be reasonable. Additionally, if a GBP frequently changes its direction like # 9, or moves from side to side with a small displacement, such as #10, these will also be categorized into the rotary motion type.

The mean velocity of all motion types is 1.77 km s^{-1}. Earlier studies of velocity are listed in Table 2. Our result is slightly elevated compared to previously published studies. One reason may be attributed to the data, with different spatial and temporal resolution/sampling across the various studies, and the fact that GBPs are identified with different methods in each of the studies (Utz et al. 2010). Utz et al. (2010) reported 1–2 km s^{-1} for different spatial and temporal sampling, and indicated that a higher spatial and temporal resolution results in a higher velocity. Another reason may be that some GBPs described in Section 3 and stationary GBPs with $m' < 1$ are not counted. If all isolated GBPs are counted, the mean velocity is 1.66$\pm$0.07 km s^{-1}.

The velocities of GBPs for the different motion types are separately calculated and compared in this study. The means and standard errors are $2.18\pm0.08\,\mathrm{km\ s^{-1}}$ for the straight motion type, $1.63\pm0.09\,\mathrm{km\ s^{-1}}$ for the erratic motion type and $1.33\pm0.07\,\mathrm{km\ s^{-1}}$ for the rotary motion type. The horizontal velocity has a notable positive correlation with the index of motion type (correlation coefficient is 0.88). Both classification and correlation analysis suggest that if a GBP moves in a straight line, it will move fast; however, if a GBP moves in a rotary path, it will move slowly. We also demonstrate that there is a significant difference between straight and rotary motion types by a two-sample K-S test. Importantly, GBPs with higher velocity ($> 2\,\mathrm{km\ s^{-1}}$) have been linked to the production of magnetosonic kink waves (de Wijn et al. 2009). As shown previously, these kink waves can act as a conduit for imparting energy into the upper solar atmosphere. About 28% of GBPs studied exceed $2\,\mathrm{km\ s^{-1}}$. Möstl et al. (2006) measured 11.3% and Keys et al. (2014) found about 15% have velocities greater than $2\,\mathrm{km\ s^{-1}}$. Our higher proportion is probably the result of the higher velocity stated above.

The diffusion index, γ, is 1.50 ± 0.08 averaged over all non-stationary, isolated GBPs. Recent authors have agreed on a super-diffusive dynamic regime. Abramenko et al. (2011) found γ = 1.53 with high resolution TiO observations of a quiet Sun area. Chitta et al. (2012) reported γ of 1.59 for their short-lived GBPs. Jafarzadeh et al. (2014) calculated the squared-displacement of each GBP and derived $\gamma = 1.69\pm0.08$ by the distribution of the diffusion indices. Giannattasio et al. (2014) found $\gamma = 1.27\pm0.05$ and $\gamma = 1.08\pm0.11$ in network regions (at smaller and larger scales, respectively), and $\gamma = 1.44\pm0.08$ in internetwork regions. Keys et al. (2014) estimated γ of $\sim$1.2 for both a quiet region and an active region, then confirmed that the dynamic properties of GBPs arise predominately from convective motions. Our result is in qualitative agreement with recent studies of diffusion. However, in earlier studies, almost all other authors interpreted their results as indicative of normal- or sub-diffusive processes. Berger et al. (1998a) found indications of slight super-diffusivity among otherwise normal diffusive GBPs in network regions. Cadavid et al. (1999) found that although the motion of magnetic network GBPs in the photosphere is random if their lifetimes are larger than 25 minutes, GBPs with lifetimes less than 20 minutes migrate sub-diffusively. All authors suggested that estimations of the diffusion index may be affected by the temporal and spatial scales.

We find that γ is 2.13 ± 0.09 for the straight motion type, 1.82 ± 0.07 for the erratic motion type, and 0.73 ± 0.19 for the rotary motion type. The larger value of γ for straight motion type comes from the fact that these GBPs move continuously in the same direction and have more Lévy flights in their path. On average, they move faster and accelerate with time. The straight motion makes a large contribution to super or even ballistic diffusion. However, the smaller γ value associated with rotary motion type may be due to the fact that it changes its general direction and returns closer to its initial coordinates. This results in a sub-diffusive regime. The γ values of different motion types confirm that our classification method is reasonable. Similarly, Jafarzadeh et al. (2014) proposed mean-squared displacement, which can result in the mixing of different diffusive processes, and therefore calculated the trajectory of each BP and described it by a diffusion index. They categorized GBPs into different motion types based on the diffusion index.

The coefficient K indicates the efficiency of the dispersion. The K values are $850\pm37\,\mathrm{km^2\ s^{-1}}$ for the straight motion type, $331\pm24\,\mathrm{km^2\ s^{-1}}$ for the erratic motion type, and $13\pm9\,\mathrm{km^2\ s^{-1}}$ for the rotary motion type. We also measure K of all motion types as a whole for $191\pm20\,\mathrm{km^2\ s^{-1}}$. GBPs which move in straight lines experience the quickest rate of diffusion, while GBPs which move in rotary paths experience the slowest rate of diffusion. Our result confirms and furthers previous studies. Berger et al. (1998a) determined $K = 60.4\pm10.9\,\mathrm{km^2\ s^{-1}}$ for network MBPs by assuming normal diffusion (i.e. $K = sd/2d\tau$), whereas the γ value of 1.34 ± 0.06 indicates a super-diffusive regime. Utz et al. (2010) found $K = 350\pm20\,\mathrm{km^2\ s^{-1}}$. Manso Sainz et al. (2011) measured $K = 195\,\mathrm{km^2\ s^{-1}}$ for footpoints of small-scale internetwork magnetic loops. Jafarzadeh et al. (2014) found $K = 257\pm32\,\mathrm{km^2\ s^{-1}}$ averaged over all MBPs. Giannattasio et al. (2014) estimated that the diffusivity increases from $\sim$ 100 to $\sim 400\,\mathrm{km^2\ s^{-1}}$ along the time scales ($100\,\mathrm{s} < \tau < 10000\,\mathrm{s}$).

The sources of such a large range could be the result of different features (magnetic elements, bright points), different regions (quiet region, active region), and/or different temporal and spatial scales, etc.

The distribution of the directions of motion of GBPs that move in straight lines show no particular preferential flow direction. It is homogeneous and isotropic. Verma & Denker (2011) adapted LCT to measure horizontal flow fields of GBPs and other features. Keys et al. (2014) tracked the motions of GBPs for exploring preferential flow directions. Our result is in agreement with them. In addition to this result, we also confirm the conclusion of Nisenson et al. (2003) and Bodnárová et al. (2014) in that the direction of motion usually persists between neighboring frames. Both studies utilized G-band images taken with the Dutch Open Telescope with a temporal sampling of 30 s. We strengthen their claim using the G-band images acquired from the *Hinode*/SOT with a temporal sampling of 11 s. Additionally, we have discussed that the kurtoses of the distributions in the three motion types are different. The kurtosis is leptokurtic for the straight motion type and platykurtic for the rotary motion type. That means a GBP, which moves in a straight line, is more likely to keep its direction than a GBP which moves along a rotary path.

Acknowledgements The authors are grateful to the anonymous referee for their constructive comments and detailed suggestions for this manuscript. The authors are grateful to the support from the National Natural Science Foundation of China (Grant Nos. 11303011, 11263004, 11163004 and U1231205), and the Open Research Program of the Key Laboratory of Solar Activity of the Chinese Academy of Sciences (Grant Nos. KLSA201414 and KLSA201309). This work is also supported by the Opening Project of the Key Laboratory of Astronomical Optics & Technology, Nanjing Institute of Astronomical Optics & Technology, Chinese Academy of Sciences (No. CAS-KLAOT-KF201306) and the open fund of the Key Laboratory of Modern Astronomy and Astrophysics, Nanjing University, Ministry of Education, China. The authors are grateful to the *Hinode* team for the use of their data. *Hinode* is a Japanese mission developed and launched by ISAS/JAXA, collaborating with NAOJ as a domestic partner, and NASA and STFC (UK) as international partners. Scientific operation of the *Hinode* mission is conducted by the *Hinode* science team organized at ISAS/JAXA. This team mainly consists of scientists from institutes in the partner countries. Support for the post launch operation is provided by JAXA and NAOJ (Japan), STFC (U.K.), NASA (U.S.A.), ESA and NSC (Norway).

References

Abramenko, V. I., Carbone, V., Yurchyshyn, V., et al. 2011, ApJ, 743, 133
Balmaceda, L., Vargas Domínguez, S., Palacios, J., Cabello, I., & Domingo, V. 2010, A&A, 513, L6
Berger, T. E., Löfdahl, M. G., Shine, R. A., & Title, A. M. 1998a, ApJ, 506, 439
Berger, T. E., Löfdahl, M. G., Shine, R. S., & Title, A. M. 1998b, ApJ, 495, 973
Bodnárová, M., Utz, D., & Rybák, J. 2014, Sol. Phys., 289, 1543
Bonet, J. A., Márquez, I., Sánchez Almeida, J., Cabello, I., & Domingo, V. 2008, ApJ, 687, L131
Cadavid, A. C., Lawrence, J. K., & Ruzmaikin, A. A. 1999, ApJ, 521, 844
Carlsson, M., Hansteen, V. H., & Gudiksen, B. V. 2010, Mem. Soc. Astron. Italiana, 81, 582
Chitta, L. P., van Ballegooijen, A. A., Rouppe van der Voort, L., DeLuca, E. E., & Kariyappa, R. 2012, ApJ, 752, 48
Cranmer, S. R. 2002, Space Sci. Rev., 101, 229
Cranmer, S. R., & van Ballegooijen, A. A. 2005, ApJS, 156, 265
de Wijn, A. G., Stenflo, J. O., Solanki, S. K., & Tsuneta, S. 2009, Space Sci. Rev., 144, 275
Fedun, V., Shelyag, S., & Erdélyi, R. 2011, ApJ, 727, 17
Feng, S., Ji, K.-f., Deng, H., Wang, F., & Fu, X.-d. 2012, Journal of Korean Astronomical Society, 45, 167
Giannattasio, F., Del Moro, D., Berrilli, F., et al. 2013, ApJ, 770, L36

Giannattasio, F., Stangalini, M., Berrilli, F., Del Moro, D., & Bellot Rubio, L. 2014, ApJ, 788, 137
Goode, P. R., Yurchyshyn, V., Cao, W., et al. 2010, ApJ, 714, L31
Ichimoto, K., Tsuneta, S., Suematsu, Y., et al. 2004, in Society of Photo-Optical Instrumentation Engineers (SPIE) Conference Series, 5487, Optical, Infrared, and Millimeter Space Telescopes, ed. J. C. Mather, 1142
Jafarzadeh, S., Cameron, R. H., Solanki, S. K., et al. 2014, A&A, 563, A101
Keys, P. H., Mathioudakis, M., Jess, D. B., et al. 2011, ApJ, 740, L40
Keys, P. H., Mathioudakis, M., Jess, D. B., Mackay, D. H., & Keenan, F. P. 2014, A&A, 566, A99
Klimchuk, J. A. 2006, Sol. Phys., 234, 41
Manso Sainz, R., Martínez González, M. J., & Asensio Ramos, A. 2011, A&A, 531, L9
Moll, R., Cameron, R. H., & Schüssler, M. 2011, A&A, 533, A126
Monin, A. S., & Iaglom, A. M. 1975, Statistical Fluid Mechanics: Mechanics of Turbulence (Cambridge, Mass., MIT Press)
Möstl, C., Hanslmeier, A., Sobotka, M., Puschmann, K., & Muthsam, H. J. 2006, Sol. Phys., 237, 13
Muller, R., Roudier, T., Vigneau, J., & Auffret, H. 1994, A&A, 283, 232
Nisenson, P., van Ballegooijen, A. A., de Wijn, A. G., & Sütterlin, P. 2003, ApJ, 587, 458
Shelyag, S., Keys, P., Mathioudakis, M., & Keenan, F. P. 2011, A&A, 526, A5
Shelyag, S., Mathioudakis, M., & Keenan, F. P. 2012, ApJ, 753, L22
Shelyag, S., Cally, P. S., Reid, A., & Mathioudakis, M. 2013, ApJ, 776, L4
Suematsu, Y., Tsuneta, S., Ichimoto, K., et al. 2008, Sol. Phys., 249, 197
Utz, D., Hanslmeier, A., Muller, R., et al. 2010, A&A, 511, A39
van Ballegooijen, A. A., Nisenson, P., Noyes, R. W., et al. 1998, ApJ, 509, 435
Verma, M., & Denker, C. 2011, A&A, 529, A153
Vögler, A., Shelyag, S., Schüssler, M., et al. 2005, A&A, 429, 335
Wedemeyer-Böhm, S., Scullion, E., Steiner, O., et al. 2012, Nature, 486, 505
Yang, Y.-F., Lin, J.-B., Feng, S., et al. 2014, RAA (Research in Astronomy and Astrophysics), 14, 741
Zhao, M., Wang, J.-X., Jin, C.-L., & Zhou, G.-P. 2009, RAA (Research in Astronomy and Astrophysics), 9, 933